



Band alignment of transition metal dichalcogenide heterostructuresFrancis H. Davies, Conor J. Price , Ned T. Taylor , Shane G. Davies, and Steven P. Hepplestone ^{*}
Department of Physics, University of Exeter, Stocker Road, Exeter, EX4 4QL, United Kingdom

(Received 27 April 2020; revised 9 October 2020; accepted 2 December 2020; published 15 January 2021)

Two-dimensional heterostructures and superlattices consisting of transition metal dichalcogenides offer huge potential in the next generation of optoelectronic devices. For such transition metal dichalcogenides, a predictive theory of their properties, based upon in-depth understanding of the interlayer interactions, is desirable due to the huge potential number of combinations. These weakly interacting heterobilayers provide an excellent case study to understand how interlayer interactions interfere with the Anderson/Schottky picture of band alignment at interfaces. We demonstrate here, using a combination of first principles and tight-binding methods, how the band alignment can be predicted in terms of a modified form of Anderson's rule. We explain how two physically based corrections to Anderson's rule, ΔE_T and ΔE_{IF} , are necessary for accurate band alignment prediction. We identify the interlayer interactions that affect band alignment prediction and show how these take the form of long range interactions between the d_{z^2} and/or p_z orbitals and induced fields between layers. Finally, we apply this theorem to Moiré and strained structures to predict these structures band alignment and provide a comprehensive guide to accurately predict the resultant band gap of the various transition metal dichalcogenide heterostructures.

DOI: [10.1103/PhysRevB.103.045417](https://doi.org/10.1103/PhysRevB.103.045417)**I. INTRODUCTION**

Two-dimensional (2D), or atomically thin, materials offer a high degree of customizability through their arrangement into van der Waals heterostructures. This is desirable because it allows a wide range of fixed material parameters to be tailored by the interface physics. This in turn leads to new properties [1], which are a result of the combined heterostructure. These van der Waals heterostructures are breaking new ground in applications such as high ZT thermoelectrics [2,3], highly efficient photodetectors [4], and photovoltaic cells [5]. A further unique feature of heterostructures that has caught considerable attention are interlayer excitons, particularly in transition metal dichalcogenide (TMDC) heterostructures for optoelectronics [6–10]. This is in part due to the spatial separation of electron-hole pairs [11]. The fundamental physics driving these applications would benefit from having a predictive approach allowing one to estimate the key properties of the heterostructure such as the band gap, and a more detailed understanding of the interface physics is determined by the band alignment and interactions of the constituents. The interface physics of these 2D heterostructures has been of intense focus, with several measurements [5–8,11–20] and theoretical calculations [10,21,22]. However, given the greater than 5000 2D materials and hence 16 million combinations [23], a predictive approach made using only the properties of the constituents is vital.

Fundamentally, the band alignment of two-dimensional heterostructures is of great interest. However, different approaches have been adopted to explain band alignment in these systems. Many use Anderson's rule, despite it being

a macroscale approach, directly or implicitly for TMDCs to determine the band alignments [5,11,13,14,20,21,24], and it has even been reported that Anderson's rule is exact for these systems [14]. Conversely, those working with 3D materials, or conventional heterostructures, have long cited that Anderson's rule fails for these systems [25–27]. The origin of this contradiction provides an opportunity to develop a fuller understanding of band alignment in all these structures. Unlike in macroscale interfaces, where the materials can be expected to adopt their bulk properties far from the interface, these 2D materials are typically one nanometer in thickness meaning such bulk methodologies would be expected to fail.

Anderson suggested (as well as Schottky Mott) that band alignment depended purely on the relative work-function/affinities of the two constituents. However, relatively few experimental systems have validated this approach. This model was expanded [28] upon thereafter to include the effect of charge states at the interface. These states are a result of (a) the formation of new states due to chemical bonding between the two systems and (b) a requirement for charge neutrality caused by the induced field created from the resultant electron affinities of the two systems [29]. These charge states include interface (or metal) induced gap states, IIGS (or MIGS) [30,31]. Predicting the energies of these states, and the shape of the electrostatic field induced across the interface, is nontrivial due to the atomic bonding and system geometry. The recent exploration [5,11,13,14,20,21] of weakly interacting two-dimensional materials offers a chance to revisit the understanding of band alignment in these systems, as unlike in the 3D case, dangling bonds are not present at the surface and new bonds are not formed between the layers, nor is substantial reconstruction present [32]. Effectively, these TMDC heterostructures are the closest real world likenesses to Anderson's original thought experiment, where the band

^{*}S.P.Hepplestone@exeter.ac.uk

alignment results from bringing two separate systems close together from infinity with minimal interaction [25]. These interactions (such as IIGS) should be more clearly identifiable in such systems and thus provides a window to enhancing our understanding of how the band alignment is governed.

In this paper we explain how band alignment in TMDC heterostructures is governed, providing insight into why Anderson's rule appears exact in some cases and fails in others. We determine how these differences arise based on the interactions of the atomic wave functions and the induced electric field due to the difference in the hole affinities of the constituents. From this, we derive analytical expressions that can be applied to predict the band gap in TMDC van der Waals heterostructures. Our methodology comes from a combination of first principles density functional theory and analytical modeling based upon tight binding. The final expression given provides a method to estimate the band alignment of these heterostructures, alleviating the necessity of large scale numerical simulations. Finally, we discuss how the theory accounts for strain and Moiré systems and how such a theory could be extended to all 2D heterostructures.

II. METHODOLOGY

To investigate 2D TMDC heterostructures and their interactions, we employ an analytical model developed using tight-binding and *ab initio* methods. This model utilizes density functional theory to calibrate and validate it. For our *ab initio* calculations, we use the PBE [33] and HSE06 [34] functionals with PAW pseudopotentials [35] and Grimme-D3 [36] correction as implemented in VASP [37]. For our density functional calculations, a plane-wave cutoff of 900 eV is used to accurately capture the confinement effects. Simulations with cutoffs of 600 eV and below showed changes in the electronic structure, which converged at 600 eV and higher. For our consideration of the Monkhorst-Pack grid [38] used in the simulations, we applied a minimum of $15 \times 15 \times 15$ for bulk TMDCs and a $15 \times 15 \times 1$ (or greater) Monkhorst-Pack grid for monolayer TMDCs. For Moiré cells, a k -point density greater than $12 \times 12 \times 1$ per monolayer constituent cell is maintained. Bulk TMDCs consisted of two three-atom individual layers in the 2H structure. Similarly, our monolayers consisted of a single layer of three atoms in H structure. Our heterostructures are formed from two of these primitive cells with H-type stacking. To generate Moiré structures we used ARTEMIS [39]. This allows the generation of supercells with a lattice matching of 12 MoS₂ cells to 13 CrS₂ cells with an angle $\sim 16.1^\circ$ and 19 MoS₂ cells to 16 HfS₂ cells with an angle $\sim 23.4^\circ$ between their respective primary lattice vectors. The structures began with an interatomic distance smaller than the average of the two bulks and were allowed to relax. In all the systems considered, we used a 15 Å vacuum gap between monolayer and bilayers to avoid spurious interactions with periodic replicas. All structures are relaxed using the conjugate gradient algorithm to within 0.001 eV/Å. Also, to avoid the effect of electric fields across the vacuum created by the charge transfer involved in the heterostructures, we created mirror image structures which were compared with to ensure the electric field effects were negligible in all cases. The bilayer structures maintain their lack of inversion symmetry

and therefore band splitting due to spin orbit coupling (SOC) still occurs [40,41]. However, here SOC is neglected as it is an intralayer effect [42] with no influence on the interlayer coupling [43] and has no direct effect on the band alignment. All relevant systems have been examined with SOC to confirm this conclusion.

III. RESULTS AND DISCUSSION

A. Band structure of TMDC heterostructures

A broad set of TMDCs are investigated using the PBE functional. In Fig. 1 we can observe the full band structure of nine TMDC heterostructures compared to their individual constituents. For many of the heterostructures the overlay bands appear to match their constituents almost exactly. The fact that this similarity is so strong could help explain why Anderson's rule is so commonly used in literature [5,11,13,14,20,21,24]. Despite this however, there are key differences that can be identified between the bands of the heterostructure and the constituents. Two clear alterations to the bands occur when a heterostructure is formed. Firstly, there is a static shift in some of the bands and, secondly, there is an interaction that drives up the valence band maximum at the Brillouin zone center (Γ). These two changes are the only significant adaptation to the Anderson's rule prediction. The limited variation and consistency of these subtle effects in the band structure make truer band-gap prediction for TMDC heterostructures attainable.

We examine in further detail two subcases considered using the more accurate HSE06 functional. We present in Fig. 2 the band alignment of WSe₂/MoS₂ and MoS₂/CrS₂, and we show that, while Anderson's rule is a reasonable estimate, it is not precisely held. This is just as was found using the PBE functional. The results in Fig. 2 show that the deviation from Anderson's rule is 0.07 eV (8.0%) for WSe₂/MoS₂ and 0.12 eV (11.9%) for MoS₂/CrS₂.

The two heterobilayers WSe₂/MoS₂ and MoS₂/CrS₂, are laterally strained resulting in a 1.90% compression on WSe₂ and 1.92% expansion on MoS₂, for the WSe₂/MoS₂ heterobilayer, and a 2.14% compression on MoS₂ and 2.53% expansion on CrS₂, for the MoS₂/CrS₂ heterobilayer. This is because TMDC heterostructures are typically incommensurate and thus the creation of a periodic unit cell inevitably results in strain. Despite this, it is still possible to distinguish interlayer and strain effects. Our calculations show the effects of strain can be treated as decoupled from the interlayer interactions. We further discuss the effects of strain on our theory later.

B. Band alignment theory

The band structures in Fig. 1 and 2 show two consistent deviations from Anderson's rule. As such, two factors are needed to correct for these deviations. These corrections are (i) ΔE_Γ , the change in the valence band energy at Γ created due to interlayer interaction (an IIGS effect) and (ii) ΔE_{IF} , the energy shift in all the bands of the constituent with the smallest hole affinity created due to the induced field.

First we discuss the role of IIGS, that is the change in the band structure due to interlayer interactions. Adjacent

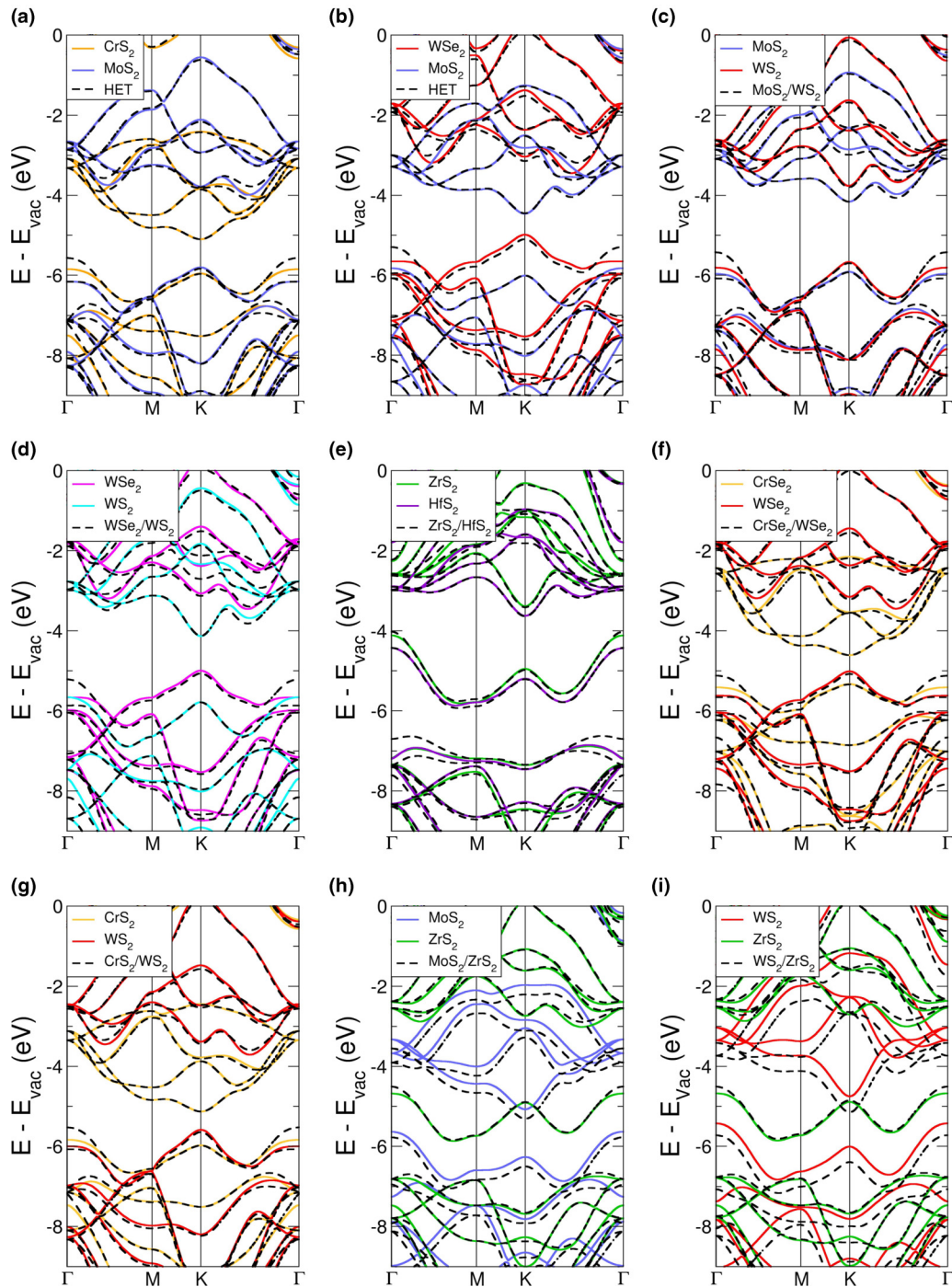


FIG. 1. The overlay band structures of all nine studied heterobilayers. From (a) to (i) they are (a) CrS₂/MoS₂, (b) WSe₂/MoS₂, (c) MoS₂/WS₂, (d) WSe₂/WS₂, (e) ZrS₂/HfS₂, (f) CrSe₂/WSe₂, (g) CrS₂/WS₂, (h) MoS₂/ZrS₂, (i) WS₂/ZrS₂. Each panel consists of the band structure of the heterostructure and the individual constituents and are aligned by reference to the vacuum level.

layers interact through weak transient bonding resulting in small distortions to the existing bands. These distortions are shown in Figs. 2(a) and 2(b), where ΔE_{Γ} equals 0.43 eV and 0.36 eV for WSe₂/MoS₂ and MoS₂/CrS₂, respectively. In the WSe₂/MoS₂ ΔE_{Γ} does not raise the valence band at Γ above the height of the valence band at K . Similarly, one can observe that the induced shift in the heterobilayer bands due to band alignment, ΔE_{IF} , is equal to 0.11 eV, for WSe₂/MoS₂ and acts on the WSe₂ bands. The deformation of the band

structure by ΔE_{Γ} is highlighted in Fig. 2(b), while Fig. 2(a) shows $\Delta E_{\Gamma} - \Delta E_{IF}$. In the MoS₂/CrS₂ case, the value of ΔE_{IF} is very small, resulting in the MoS₂ bands being shifted by 0.03 eV in the heterobilayer. This shift is driven by an induced field created from the relative positions of the two constituents' valence bands. It is interesting that our results show that correction due to charge transfer resulting from the band offset is nonlinear, as has been suggested in previous works [44]. This, in turn, suggests that the electric field does

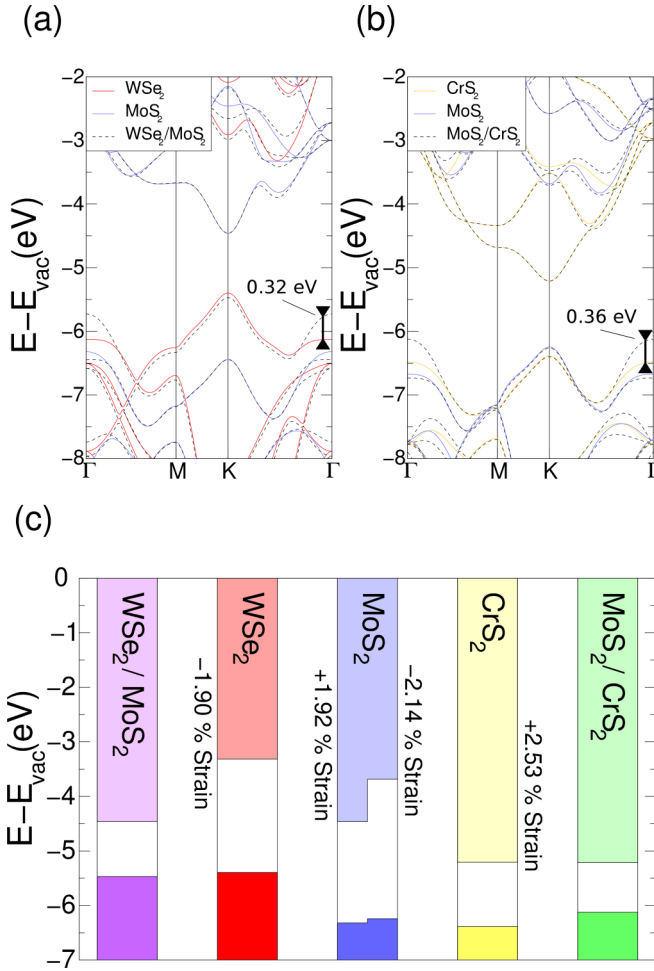


FIG. 2. (a) The electronic dispersion of the heterostructure WSe₂/MoS₂ (black dashed) overlaying the electronic dispersions of the two constituents WSe₂ (red) and MoS₂ (blue). (b) Dispersion of the heterostructure MoS₂/CrS₂ (black dashed) overlaying the electronic dispersions of the MoS₂ (blue) and CrS₂ (yellow). (c) Band edge diagram of heterostructures and their constituents showing VBM and CBM. All energies are plotted relative to the vacuum energy and calculated with the HSE06 functional.

not follow the simple quadratic form normally considered for a heterojunction.

1. Induced field correction, ΔE_{IF}

The shift in band alignment due to the field induced from the band offset can be described as ΔE_{IF} . The simulation data for ΔE_{IF} is plotted against the VBM offset ($\chi_{h,B} - \chi_{h,A}$) in Fig. 1. ΔE_{IF} is defined as the average band shift for all k points along the band edge from M to K. Figure 3 shows the empirical fit

$$\Delta E_{IF} = \alpha (\exp(\beta (\chi_{h,B} - \chi_{h,A})) - 1), \quad (1)$$

where α and β are 0.03 eV and 1.91 Å/eV, respectively. We define material A as having the smaller hole affinity, $\chi_{h,A}$, compared to the hole affinity of material B, $\chi_{h,B}$. The form of Eq. (1) both agrees with the data and obeys the condition $\Delta E_{IF} = 0$ for identical layers (i.e., a bilayer system consisting of a single material).

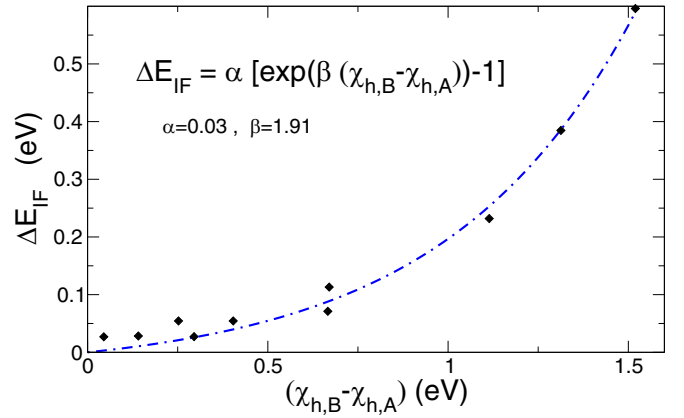


FIG. 3. The relationship between the valence band offset ($\chi_{h,B} - \chi_{h,A}$) and the resultant shift in the band energies (ΔE_{IF}). The inset gives the equation and parameters for the empirical fit (blue dashed line).

The shift, ΔE_{IF} , is similar to the description of band bending in conventional heterostructures created by a charge transfer that occurs due to the VBM offset, which induces an electric field. However, the functional form of the electric field is not simply described. Its effect is to change the relative energy of the bands in each layer such that local electron affinity is preserved. The resultant electric field also changes the vacuum energy in that region. By defining the highest local potential energy as the vacuum, we observe that the lower valence band material (negatively charged, so higher vacuum energy) is aligned with the heterobands and the other layer has shifted bands. This shift is the term we describe as ΔE_{IF} . As expected, this induced field does not change the size of the band gap of either constituent as has been observed in monolayer systems [45].

The effect of ΔE_{IF} on the bands is constant however how it effects the band gap depends on the band alignment. In type II band alignment (where the two band gaps partially overlap), the effect of ΔE_{IF} will be to increase the band gap since the VBM will drop lower. In the case of type I band alignment (where one constituents band gap lies completely within the other material), the heterobilayers will have an unchanged band gap because both the VBM and conduction band minima (CBM) change together. Hence, from Eq. (1) it is possible to determine the shift, ΔE_{IF} , based only on the properties of the monolayer constituents.

2. Layer hybridization correction, ΔE_{Γ}

We have explored one of the identified consistent deviations from Anderson's rule, and a second corrective term, arising from the overlap of the atomic wave functions between layers, is required, which we describe as ΔE_{Γ} . This shift can be seen in Figs. 2(a) and 2(b) at Γ , as well as many of the band structures in Fig. 1. This shift will usually, but not always, affect the band gap, depending on where the VBM is located in the Brillouin zone. When the valence band at Γ , $E_{VB}(\mathbf{k} = \Gamma)$, is below the VBM, E_{VBM} , by an amount greater than ΔE_{Γ} , then the band gap will not be affected. As is the case in Fig. 2(b), we find that, typically, $\Delta E_{\Gamma} >$

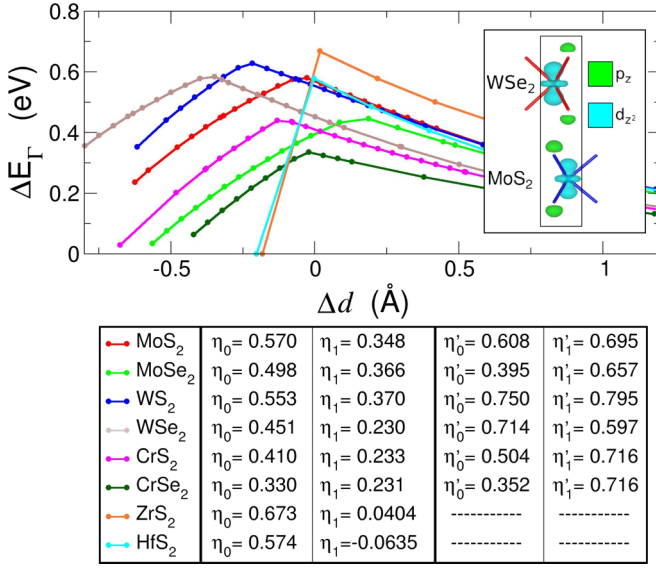


FIG. 4. (Top) The relation between ΔE_{Γ} and Δd . (Bottom) The tabulated fitting parameters that reproduce the simulation data, corresponding to those in Eq. (2) for η_0 (eV) and η_1 (eV/Å). Both ZrS₂ and HfS₂ are metallic for $d \leq 6$ Å and therefore have no η'_i values.

($E_{\text{VBM}} - E_{\text{VB}}(\mathbf{k} = \Gamma)$) and thus it reduces the band gap of the heterostructure.

The ΔE_{Γ} term comes from the weak overlap of the orbitals of the two constituent layers. To examine this behavior, we have calculated the magnitude of ΔE_{Γ} using first principles simulations by varying the interlayer spacing d in bulk TMDCs, as shown in Fig. 4. Analysis of the projected density of states suggests that the magnitude of ΔE_{Γ} is controlled by the overlap of the $\langle d_{z^2} | d_{z^2} \rangle$ and $\langle p_z | d_{z^2} \rangle$ (which is a function of d). The sharp discontinuity corresponds to the switch between energy configurations, i.e., from $\langle d_{z^2} | d_{z^2} \rangle$ to $\langle p_z | d_{z^2} \rangle$. To confirm this, we have developed a tight binding model [46–48], calibrated from our first principles findings. In this model, we have shown that, while the in-layer components consist of d_{xy} and $d_{x^2-y^2}$, we only need to consider the interactions of the p_z and d_{z^2} orbitals between layers to replicate the behavior of ΔE_{Γ} . In agreement with previous work we dismiss the weaker π and δ bonding as insignificant interlayer contributions [49]. These results show that ΔE_{Γ} is driven by the bonding and antibonding interaction of the p_z and d_{z^2} orbitals between layers. Generally, the tight-binding approach clearly shows that the p_z - d_{z^2} (d_{z^2} - d_{z^2}) dominates in the high (low) separation regimes. We note, however, for HfX₂ and ZrX₂ the behavior is controlled by $\langle p_z | p_z \rangle$, which becomes metallic at low separations. This is due to these nanostructures effectively having their d orbitals depleted to form the TMDC structure. Furthermore, the splitting is no longer meaningful beyond the point that the nanostructure becomes metallic.

Following our tight-binding model, we derive a simplified form for ΔE_{Γ} by directly considering the overlap of $\langle d_{z^2} | p_z \rangle$ or $\langle d_{z^2} | d_{z^2} \rangle$. This suggests ΔE_{Γ} should take the form

$$\Delta E_{\Gamma} = e^{-\lambda \Delta d} \sum_{i=0}^{n+n'-3} \eta_i (\Delta d)^i, \quad (2)$$

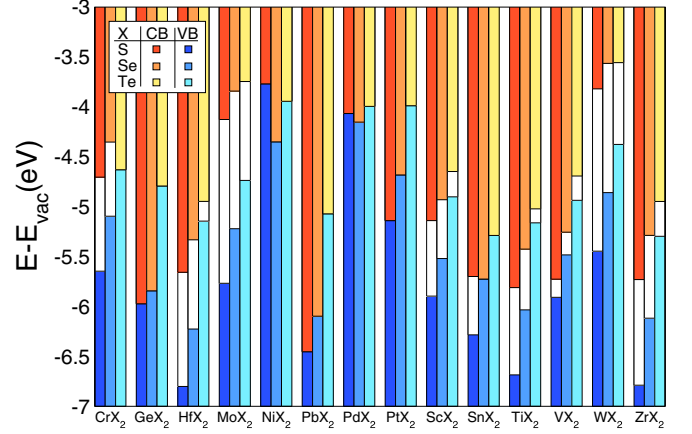


FIG. 5. Conduction and valence band edges calculated within PBE for the 2D TMDCs. The colored bar edges represent the valence bands (shades of blue/cyan) and the conduction bands (shades of red/yellow) for each monolayer; all energies are taken with respect to the vacuum level. Due to the band gap underestimate by PBE, the electron affinities are overestimated.

where Δd is the change in separation from the bulk interlayer spacing, defined as $d - d_0$, with d_0 being the bulk interlayer spacing and d the interlayer spacing of the hetero/homobilayer. λ and η_i are constants, which differ for the p_z - d_{z^2} or d_{z^2} - d_{z^2} regimes with n and n' being principle quantum numbers. One can estimate the value of λ and η_i using the 2H-TMDCs (η_i in the p_z - d_{z^2} regime and where η'_i denotes the d_{z^2} - d_{z^2} regime). Hence, we have evaluated ΔE_{Γ} for many 2H-TMDCs at different spacings (d), using the PBE functional, as shown in Fig. 4. From these results, we determine that $\lambda = 1.3$ Å⁻¹ ($\lambda' = 0.5$ Å⁻¹) with the exception of those 2D layered materials which are p_z - p_z dominated (ZrS₂ and HfS₂) where $\lambda = 0.75$ Å⁻¹. The values of η_i for Eq. (2) are given in Fig. 4. The first two terms are sufficient to make the error of Eq. (2) negligible ($\sim 10^{-5}$ eV) compared with the simulation data.

The remaining parameters are material dependent and can now be evaluated using the appropriate values for λ and η_i and the interlayer distance. The interlayer distance can be approximated as the average of the distances between the layers in the two bulk constituents. Now, one only has to consider the higher VBM material and use Eq. (2) with that materials parameters and the average interlayer spacing to estimate ΔE_{Γ} .

3. Band-gap prediction

Having evaluated the corrections to Anderson's rule, we propose a corrected form which calculates the band offsets using only information about the monolayer constituents. We present the key properties, the band edges, of the monolayer constituents in Fig. 5.

The two corrections explored in this work can be implemented on top of an Anderson's approach. It is first necessary to evaluate whether the system is type I, II, or III. This is determined from the electron and hole affinities, χ_e and χ_h , respectively. By defining material A using the condition $\chi_{h,A} > \chi_{h,B}$, it is possible to define the type of

TABLE I. Tabulated values of TMDC heterobilayers quantitatively comparing the original and corrected Anderson's band-gap predictions to the DFT PBE band-gap values. The values of ΔE_{Γ} and ΔE_{IF} are calculated using Eq. (1) and Eq. (2), respectively. Here ΔE_{VB} equals $E_{\text{VBM}} - E_{\text{VB}}(\mathbf{k} = \Gamma)$ and d is the interlayer spacing. The error values of the corrected method are directly compared to those obtained using Anderson's rule. Heterobilayers in this table without provided error values have type III band alignment and are therefore metallic.

Hetero	ΔE_{VB} (eV)	ΔE_{Γ} (eV)	ΔE_{IF} (eV)	d (Å)	Band gap (eV)			Error	
					DFT	Anderson's	Corrected	Anderson's	Corrected
CrS ₂ /MoS ₂	0.045	0.378	0.003	6.15	0.465	0.700	0.343	50.71%	20.90%
WSe ₂ /MoS ₂	0.670	0.537	0.078	6.37	0.647	0.521	0.641	19.41%	7.36%
MoS ₂ /WS ₂	0.141	0.342	0.009	6.22	1.260	1.505	1.107	19.51%	4.27%
WSe ₂ /WS ₂	0.666	0.536	0.077	6.37	0.936	0.858	0.941	8.33%	0.09%
ZrS ₂ /HfS ₂	0.295	0.656	0.023	6.22	0.696	1.021	0.683	46.67%	1.89%
CrSe ₂ /WSe ₂	0.404	0.102	0.035	6.48	0.468	0.398	0.438	15.00%	7.54%
CrS ₂ /WS ₂	0.252	0.371	0.019	6.17	0.393	0.451	0.301	14.85%	15.43%
MoS ₂ /ZrS ₂	1.114	0.594	0.083	6.18	0.000	0.000	0.000		
WS ₂ /ZrS ₂	1.313	0.340	0.113	6.22	0.000	0.000	0.000		
Average								24.93%	8.21%
Standard deviation								16.70%	7.48%

heterostructure following the normal convention, i.e., type I alignment if $\chi_{e,B} > \chi_{e,A}$, type III if $\chi_{e,A} > \chi_{h,B}$, type II otherwise. The ΔE_{IF} correction will only affect the band gap for type II band alignments. It is also necessary to determine to what extent ΔE_{Γ} will affect the band gap. As discussed earlier, ΔE_{Γ} must be larger than $(E_{\text{VBM}} - E_{\text{VB}}(\Gamma))$ to alter the band gap, and generally this is the case. This requires the difference in energies for the valence band at Γ , $E_{\text{VB}}(\Gamma)$, and the valence band maxima (normally at K), E_{VBM} . We implement the positive part function, which express the band-gap reduction due to ΔE_{Γ} as

$$E'_{\Gamma} = \frac{\Delta E_{\Gamma} - (E_{\text{VBM}} - E_{\text{VB}}(\Gamma))}{2} + \frac{|\Delta E_{\Gamma} - (E_{\text{VBM}} - E_{\text{VB}}(\Gamma))|}{2}. \quad (3)$$

Hence, we can evaluate the band gap of the heterostructure. For type I, it is expressed as

$$E_g = \chi_{e,B} - \chi_{h,B} - E'_{\Gamma}, \quad (4)$$

and for type II

$$E_g = \chi_{e,B} - \chi_{h,A} + \Delta E_{\text{IF}} - E'_{\Gamma}, \quad (5)$$

and for type III $E_g = 0$. This approach reduces the mean error in predicting the band gap of a heterostructure using Anderson's rule (approximately 25%) to less than 10%.

A complete quantitative comparison between the *ab initio* simulation data (from Fig. 1) and the predictive band-gap theory is included in Table I. It shows that the corrected values of Anderson's rule have a reduced error on average. The greatest reduction is given by ZrS₂/HfS₂ and the only system for which the corrected prediction is worse is CrS₂/WS₂. The average error in band-gap prediction falls below 10% when applying the corrections. Conversely Anderson's rule has an average error above 24%. This demonstrates the advantages of applying the corrected theory over the current Anderson's rule approach. Furthermore, with the standard deviation of the corrected rule being approximately half that of Anderson's rule,

there is significantly more reliability that the corrected rule will, for a given heterostructure pairing, provide a reasonable band-gap prediction.

Corrected rule band gaps can be calculated by applying Eqs. (3), (4), and (5) alongside the Table I values for ΔE_{VB} , ΔE_{Γ} , ΔE_{IF} , and Anderson's band gap. When the heterobilayer is of type I band alignment, the Anderson's rule prediction for the band gap is equivalent to $(\chi_{e,B} - \chi_{h,B})$ from Eq. (4). When the heterobilayer is of type II band alignment, Anderson's rule is $(\chi_{e,B} - \chi_{h,A})$ from Eq. (5). The value of d is the interlayer distance, however, the average of the constituents can be used with a mean error of 1.87%. Calculation of the band gaps depends on using the appropriate equation for the respective band alignment; CrS₂/MoS₂ and CrS₂/WS₂ are of type I, MoS₂/ZrS₂ and WS₂/ZrS₂ are of type III, and all others are of type II.

C. Discussion of Moiré and strain effects on band alignment

Thus far all discussions have included strained TMDCs with no rotation between layers. This is a product of the one-to-one cell matching. The assumption that the effects of strain are additive to the effects of interlayer interaction is reasonable. The basis of this assumption is that if a strained TMDC constitutes part of the heterostructure then that constituent is not MX₂ but is instead strained MX₂. At first, this would appear to undermine the empirical band-gap prediction presented in this paper as it would require exact knowledge of the strain characteristics of each TMDC, both when in a heterostructure and when in isolation. This would, once again, require the application of density functional theory and hence one might as well calculate the heterostructure itself. However, real world TMDCs tend to form heterostructures with incommensurate lattice matching resulting in a Moiré lattice pattern. A greater concern of Moiré structures is how rotated lattices will affect the interlayer interaction.

Through the examination of Moiré lattice heterostructures, testing the assumption that strain is additive with the

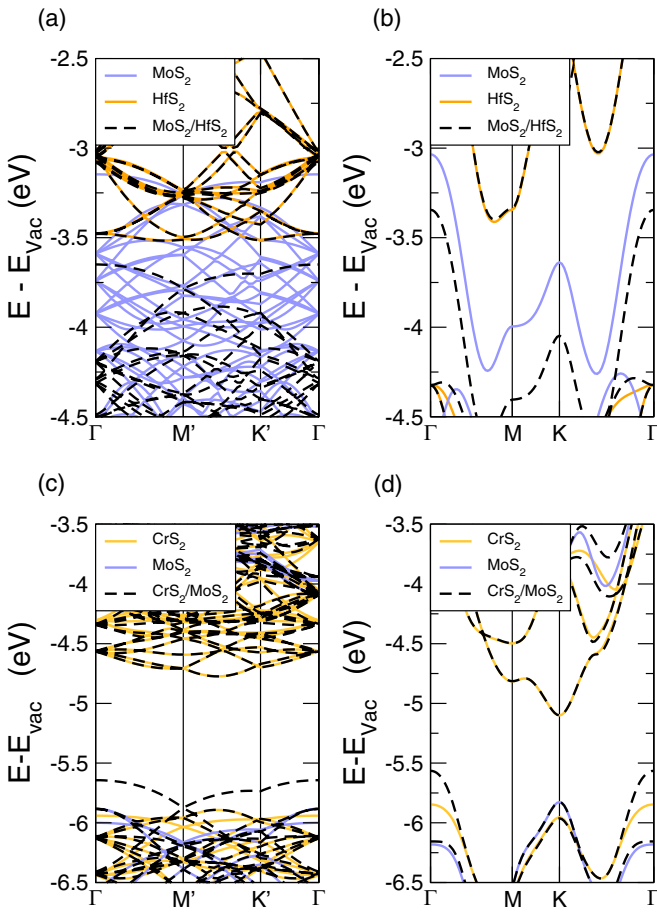


FIG. 6. (a),(b) An overlay band structure showing the constituent bands (blue and orange) overlaid by the heterobilayer bands (black dashed) with (a) showing the Moiré structure and (b) showing the one-to-one cell matching for MoS₂/HfS₂. (c),(d) Constituent bands (blue and gold) with heterobilayer bands (black dashed) overlaid. (c) Showing the Moiré structure and (d) showing a one-to-one cell matching for CrS₂/MoS₂.

interlayer interaction is easily done, since the Moiré structures are effectively without strain (average strain <1%). It is also possible to investigate the effects of rotation. For this purpose two heterostructures have been examined. Calculations for MoS₂/HfS₂ and CrS₂/MoS₂ Moiré structures were performed using the same methodology as the lattice matched heterostructures.

It can be observed from Figs. 6(a) and 6(b) that both Moiré and lattices matched systems have a significant ΔE_{IF} . However comparison between the two requires careful consideration of their relative strains. Because the strain on the constituents changes between the two systems it is necessary to test them against our identified trend instead of against each other. In the case of MoS₂/HfS₂ Moiré structure the value of ΔE_{IF} is 0.596 eV for a band offset of 1.520 eV; this deviates from Eq. (1) by 0.07 eV. The one-to-one MoS₂/HfS₂ heterobilayer results in $\Delta E_{\text{IF}} = 0.346$ eV, for a band offset of 1.284 eV, deviating from Eq. (1) by 0.02 eV. This demonstrates that Moiré twisting and strain do not effect the validity of Eq. (1).

It is expected that ΔE_{IF} is preserved as it does not depend on the local structure. It depends on the relative VBM heights across each layer. The effect on ΔE_{Γ} however is dependent on the local atomic positioning between the two layers. The nature of an incommensurate Moiré lattice is that it will, at some point, pass through all local configurations. By this logic, the vertical atomic alignment giving rise to the $\langle d_z^2 | p_z \rangle$ interaction must occur within the structure. If this interaction is present anywhere in the system, it will represent the band with the highest energies at Γ .

Figures 6(c) and 6(d) show the effect of Moiré twisting and strain on ΔE_{Γ} . In spite of the changing strain on the systems, the change in ΔE_{Γ} is less than 0.02 eV. This change is a direct result of the strain of the components and not the angle twist. Hence, the Moiré lattice has no important effect on the band alignment rule for the minimal gap presented in Eqs. (4) and (5). However, a significant feature that arises from the Moiré twisting is the band folding. Due to the reduced periodicity, the symmetry breaking bands become folded back across the Brillouin zone. This would mean for optical processes there would be more direct transitions. This could be observed through a reduction in thermalization during electro/photoluminescence.

In considering TMDC heterostructures, often strain is the first practical concern. These effects have been thoroughly explored over the last decade [4,15,47,50–54], which provides a guide to incorporating the effects of strain into the above methodology. An effective tight-binding model proposed by Pearce *et al.* [47] provided a fundamental description of how strain influences the electronic response and key points in the band structure. In addition, several groups have applied first principles techniques to explore the role of strain. Johari and Shenoy [51], in 2012, gave an exploration of lateral strain effects in MoX₂ and WX₂ (where X= S, Se, Te) using first principles. These results can be used to determine the band-gap changes of these constituents for strains of up to 10%. Rasmussen and Thygesen [53] provide details for in-plane strains of up to 2%, covering all feasible TMDC structures, which can be used to extract the band-gap behavior. The effects of strain have also been explored extensively by Kang and Kwon [55] computationally showing the band gap with the PBE approximation for differing values of strain for various TMDC sulphides and selenides (M = Mo, W, Ti, Cr, V, Nb, Ta, Hf, Zr) and show that the trends hold when considered using the GW method, while experiment has shown that these structures can sustain higher strains than conventional materials [54] (up to 10%). However, heterostructures formed from 2D materials show much lower or no strain [14–19], due to the weak interlayer interaction meaning that there is no pinning of adjacent layer positions. If one wishes to include the effects of strain in the theory discussed, then one could consider the results presented in the above works and use these to scale the band gap, and then apply the corrective terms, ΔE_{Γ} and ΔE_{IF} . In these cases, we expect that ΔE_{Γ} and ΔE_{IF} would be overestimates but not sufficiently different to prevent a reasonable estimate of the band gap, which can be confirmed by comparison of our results with Lu *et al.* [56]. Our results have indicated that strains of less than 5% have minimal impact on the theory presented.

D. Discussion

Experimental evidence for ΔE_Γ and ΔE_{IF} relies on optical techniques, where one has to be careful to separate excitonic effects. However, recent measurements by Wu *et al.* [19] of WSe_2/WS_2 show that the heterostructure has a clear reduction in band gap compared to the result expected from Anderson's rule. In their report it is suggested that this is an issue with the accuracy of their measurements, but we suggest here that the reduction is due to ΔE_Γ . Similarly, Aretouli *et al.* [16] report a miscellaneous reduction in the band gap of $\text{HfSe}_2/\text{MoSe}_2$, which is evidence of the effect of ΔE_Γ . Indirect evidence of this is also observed in the exciton behavior in heterostructures [57], as the effect of ΔE_Γ is to increase the energy of the valence band at Γ and thus decrease its effective mass, resulting in the exciton lifetime being increased. The case of $\text{MoS}_2/\text{WSe}_2$ is the most discussed case [14,17,18], however it is an unhelpful candidate for experimental comparison due to the predicted correction term being negligible [see Figs. 2(a) and 2(c)]. This prediction is, however, consistent with experimental results, which would suggest for this particular pairing that Anderson's rule is obeyed [14].

The expressions Eq. (4) and Eq. (5) have interesting implications for TMDC heterostructures and for 2D materials in general. Firstly, the effective mass (and transport properties) of the valence band depends on ΔE_Γ and hence on the interaction between layers. This factor will always increase the curvature (and thus mobility) of the valence band, and this provides a mechanism to enhance the transport characteristics of the heterostructure over the constituents. Conversely, the conduction band is almost identical (see Fig. 2) to the constituent that has the highest electron affinity.

The particular orbital overlap here is unique to H-TMDCs, but due to all orbital interactions following similar forms as Eq. (2), the shift from ΔE_Γ will be universal with values of λ and η_i changing, which implies that one could expect external pressure applied perpendicularly to create a pressure sensitive band gap for all 2D heterostructures, under the condition that this shift results in Eq. (3) being nonzero. The interaction in ΔE_Γ also clearly explains the transition between direct and indirect behavior between TMDC monolayers and the bulk in terms of a simple analytically described interaction.

Type III 2D heterostructures offer an intriguing possibility compared to bulk heterostructures. Normally, when considering a heterostructure, one considers the system being in equilibrium with the bulk materials properties, forming a triangular well. In this case, as both layers are less than a nanometer thick, one can expect that one 2D layer will effectively have an empty valence band and the other will have a significantly filled conduction band. This would result in both layers being metallic, but with electron and hole conduction localized to different layers.

IV. CONCLUSION

In conclusion, we have demonstrated and explained the failure of Anderson's rule and how it can be corrected to more accurately predict 2D heterostructure band gaps. We have shown that due to ΔE_Γ any constructed heterostructure is likely to exhibit an indirect band gap and that the effective

mass will always decrease. Furthermore we have provided expressions to give the band alignments in terms of the material properties of the constituents and their separation. The theory could be readily extended to other 2D heterostructures with some minor adjustments to ΔE_Γ and ΔE_{IF} . The approach presents a method which avoids the need for advanced calculation when estimating the properties of TMDC heterostructures. This expands the possibilities for exploring the optoelectronic properties of various heterostructures to the broader community.

ACKNOWLEDGMENTS

Via our membership of the UK's HEC Materials Chemistry Consortium, which is funded by EPSRC (EP/L000202, EP/R029431), this work used the ARCHER UK National Supercomputing Service (<http://www.archer.ac.uk>). Also, all of the authors acknowledge funding from the EPSRC (EP/L015331/1). We acknowledge useful discussions with T. Chan, J. Pitfield, E. Baker, and M. Portnoi.

S.P.H. started the project. F.H.D. and S.P.H. conceived and developed the analytical expressions. F.H.D. developed the tight-binding model. F.H.D. and C.J.P. carried out *ab initio* simulations to support the analytical models. F.H.D., C.J.P., N.T.T., S.G.D., and S.P.H. analyzed and interpreted the data. F.H.D. and S.P.H. wrote the paper with input from all co-authors.

TABLE II. Tabulated comparison between literature and the constituents materials of the lattice constant a , hoe affinity χ_h , and band gap E_g applied within the main text.

		This work	Ref. [58]	Ref. [59]	Ref. [60]	Ref. [53]
CrS ₂	a (Å)	3.02				3.05
	χ_h (eV)	-5.65				-6.08
	E_g (eV)	0.94				0.90
CrSe ₂	a (Å)	3.20				3.21
	χ_h (eV)	-5.10				-5.50
	E_g (eV)	0.74				0.70
HfS ₂	a (Å)	3.53				3.54
	χ_h (eV)	-6.80				-7.05
	E_g (eV)	1.14				0.93
MoS ₂	a (Å)	3.16	3.11	3.19	3.18	3.18
	χ_h (eV)	-5.77				-6.13
	E_g (eV)	1.64		1.70	1.68	1.58
MoSe ₂	a (Å)	3.32	3.24	3.32	3.32	3.32
	χ_h (eV)	-5.22				-5.5
	E_g (eV)	1.38		1.48	1.43	1.32
WS ₂	a (Å)	3.18	3.13	3.19	3.18	3.19
	χ_h (eV)	-5.45				-5.75
	E_g (eV)	1.63		1.84	1.81	1.51
WSe ₂	a (Å)	3.32	3.25	3.32	3.32	3.32
	χ_h (eV)	-4.86				-5.13
	E_g (eV)	1.29		1.59	1.53	1.22
ZrS ₂	a (Å)	3.57				3.57
	χ_h (eV)	-6.79				-7.02
	E_g (eV)	1.06				0.84

APPENDIX

In this Appendix we present in Table II a comparison between our calculated values for the individual TMDCs and

results from the works of Akbari *et al.* [58], Saha *et al.* [59], Bhattacharyya *et al.* [60], and Rasmussen *et al.* [53]. As can be seen, the results are in very good agreement with previously published works.

-
- [1] K. S. Novoselov, A. Mishchenko, A. Carvalho, and A. H. Castro Neto, *Science* **353**, aac9439 (2016).
- [2] G. Ding, C. Wang, G. Gao, K. Yao, C. Dun, C. Feng, D. Li, and G. Zhang, *Nanoscale* **10**, 7077 (2018).
- [3] X. Zhang, D. Sun, Y. Li, G. H. Lee, X. Cui, D. Chenet, Y. You, T. F. Heinz, and J. C. Hone, *ACS Appl. Mater. Interfaces* **7**, 25923 (2015).
- [4] A. De Sanctis, I. Amit, S. P. Hepplestone, M. F. Craciun, and S. Russo, *Nat. Commun.* **9**, 1652 (2018).
- [5] J. Ahn, P. J. Jeon, S. R. A. Raza, A. Pezeshki, S.-W. Min, D. K. Hwang, and S. Im, *2D Mater.* **3**, 045011 (2016).
- [6] B. Miller, A. Steinhoff, B. Pano, J. Klein, F. Jahnke, A. Holleitner, and U. Wurstbauer, *Nano Lett.* **17**, 5229 (2017).
- [7] S. Ulstrup, A. G. Čabo, J. A. Miwa, J. M. Riley, S. S. Grønborg, J. C. Johannsen, C. Cacho, O. Alexander, R. T. Chapman, E. Springate *et al.*, *ACS Nano* **10**, 6315 (2016).
- [8] P. Rivera, H. Yu, K. L. Seyler, N. P. Wilson, W. Yao, and X. Xu, *Nat. Nanotechnol.* **13**, 1004 (2018).
- [9] A. Arora, M. Drüppel, R. Schmidt, T. Deilmann, R. Schneider, M. R. Molas, P. Marauhn, S. Michaelis de Vasconcellos, M. Potemski, M. Röhlfing *et al.*, *Nat. Commun.* **8**, 639 (2017).
- [10] E. Torun, H. P. C. Miranda, A. Molina-Sánchez, and L. Wirtz, *Phys. Rev. B* **97**, 245427 (2018).
- [11] F. Ceballos, M. Z. Bellus, H. Y. Chiu, and H. Zhao, *ACS Nano* **8**, 12717 (2014).
- [12] H. M. Hill, A. F. Rigosi, K. T. Rim, G. W. Flynn, and T. F. Heinz, *Nano Lett.* **16**, 4831 (2016).
- [13] W. Choi, I. Akhtar, M. A. Rehman, M. Kim, D. Kang, J. Jung, Y. Myung, J. Kim, H. Cheong, and Y. Seo, *ACS Appl. Mater. Interfaces* **11**, 2470 (2019).
- [14] M.-H. Chiu, W.-H. Tseng, H.-L. Tang, Y.-H. Chang, C.-H. Chen, W.-T. Hsu, W.-H. Chang, C.-I. Wu, and L.-J. Li, *Adv. Funct. Mater.* **27**, 1603756 (2017).
- [15] E. Koo, Y. Lee, Y. Song, M. Park, and S.-Y. Ju, *ACS Appl. Electron. Mater.* **1**, 113 (2019).
- [16] K. E. Aretouli, P. Tsipas, D. Tsoutsou, J. Marquez-Velasco, E. Xenogiannopoulou, S. A. Giamini, E. Vassalou, N. Kelaidis, and A. Dimoulas, *Appl. Phys. Lett.* **106**, 143105 (2015).
- [17] M.-H. Chiu, M.-W. Li, W. Zhang, W.-T. Hsu, W.-H. Chang, M. Terrones, and L.-J. Li, *ACS Nano* **8**, 9649 (2014).
- [18] M.-H. Chiu, C. Zhang, H.-W. Shiu, C.-P. Chuu, C.-H. Chen, C.-Y. S. Chang, C.-H. Chen, M.-Y. Chou, C.-K. Shih, and L.-J. Li, *Nat. Commun.* **6**, 7666 (2015).
- [19] X. Wu, X. Wang, H. Li, Z. Zeng, B. Zheng, D. Zhang, F. Li, X. Zhu, Y. Jiang, and A. Pan, *Nano Res.* **12**, 3123 (2019).
- [20] W. Wang, K. Li, Y. Wang, W. Jiang, X. Liu, and H. Qi, *Appl. Phys. Lett.* **114**, 201601 (2019).
- [21] K. Xu, Y. Xu, H. Zhang, B. Peng, H. Shao, G. Ni, J. Li, M. Yao, H. Lu, H. Zhu *et al.*, *Phys. Chem. Chem. Phys.* **20**, 30351 (2018).
- [22] B. Amin, N. Singh, and U. Schwingenschlögl, *Phys. Rev. B* **92**, 075439 (2015).
- [23] N. Mounet, M. Gibertini, P. Schwaller, D. Campi, A. Merkys, A. Marrazzo, T. Sohier, I. E. Castelli, A. Cepellotti, G. Pizzi *et al.*, *Nat. Nanotechnol.* **13**, 246 (2018).
- [24] A. Chaves, J. G. Azadani, H. Alsalman, D. R. da Costa, R. Frisenda, A. J. Chaves, S. H. Song, Y. D. Kim, D. He, J. Zhou *et al.*, *npj 2D Mater. Appl.* **4**, 29 (2020).
- [25] W. Mönch, *Semiconductor Surfaces and Interfaces* (Springer, Berlin, 1993).
- [26] K. T. Delaney, N. A. Spaldin, and C. G. Van De Walle, *Phys. Rev. B* **81**, 165312 (2010).
- [27] M. Aldegunde, S. P. Hepplestone, P. V. Sushko, and K. Kalna, *Semicond. Sci. Technol.* **29**, 054003 (2014).
- [28] V. Heine, *Phys. Rev.* **138**, A1689 (1965).
- [29] H. Kroemer, *CRC Crit. Rev. Solid State Sci.* **5**, 555 (1975).
- [30] E. Louis, F. Yndurain, and F. Flores, *Phys. Rev. B* **13**, 4408 (1976).
- [31] C. Tejedor and F. Flores, *J. Phys. C: Solid State Phys.* **11**, L19 (1977).
- [32] A. K. Geim and I. V. Grigorieva, *Nature (London)* **499**, 419 (2013).
- [33] J. P. Perdew, K. Burke, and M. Ernzerhof, *Phys. Rev. Lett.* **77**, 3865 (1996).
- [34] J. Heyd, G. E. Scuseria, and M. Ernzerhof, *J. Chem. Phys.* **118**, 8207 (2003).
- [35] G. Kresse and D. Joubert, *Phys. Rev. B* **59**, 1758 (1999).
- [36] S. Grimme, J. Antony, S. Ehrlich, and H. Krieg, *J. Chem. Phys.* **132**, 130901 (2010).
- [37] G. Kresse and J. Furthmüller, *Comput. Mater. Sci.* **6**, 15 (1996).
- [38] J. D. Pack and H. J. Monkhorst, *Phys. Rev. B* **16**, 1748 (1977).
- [39] N. T. Taylor, F. H. Davies, I. E. M. Rudkin, C. J. Price, T. H. Chan, and S. P. Hepplestone, *Comput. Phys. Commun.* **257**, 107515 (2020).
- [40] A. M. Jones, H. Yu, J. S. Ross, P. Klement, N. J. Ghimire, J. Yan, D. G. Mandrus, W. Yao, and X. Xu, *Nat. Phys.* **10**, 130 (2014).
- [41] D. Xiao, G. B. Liu, W. Feng, X. Xu, and W. Yao, *Phys. Rev. Lett.* **108**, 196802 (2012).
- [42] D. Le, A. Barinov, E. Preciado, M. Isarraraz, I. Tanabe, T. Komesu, C. Troha, L. Bartels, T. S. Rahman, and P. A. Dowben, *J. Phys.: Condens. Matter* **27**, 182201 (2015).
- [43] C. Zhang, C. P. Chuu, X. Ren, M. Y. Li, L. J. Li, C. Jin, M. Y. Chou, and C. K. Shih, *Sci. Adv.* **3**, e1601459 (2017).
- [44] W. Mönch, *J. Appl. Phys.* **120**, 104501 (2016).
- [45] T. Tian, D. Scullion, D. Hughes, L. H. Li, C.-J. Shih, J. Coleman, M. Chhowalla, and E. J. G. Santos, *Nano Lett.* **20**, 841 (2020).
- [46] K. V. Shanavas and S. Satpathy, *Phys. Rev. B* **91**, 235145 (2015).
- [47] A. J. Pearce, E. Mariani, and G. Burkard, *Phys. Rev. B* **94**, 155416 (2016).

- [48] G.-B. Liu, W.-Y. Shan, Y. Yao, W. Yao, and D. Xiao, *Phys. Rev. B* **88**, 085433 (2013).
- [49] S. Fang, R. Kuate Defo, S. N. Shirodkar, S. Lieu, G. A. Tritsarlis, and E. Kaxiras, *Phys. Rev. B* **92**, 205108 (2015).
- [50] S. Pak, J. Lee, Y.-W. Lee, A.-R. Jang, S. Ahn, K. Y. Ma, Y. Cho, J. Hong, S. Lee, H. Y. Jeong *et al.*, *Nano Lett.* **17**, 5634 (2017).
- [51] P. Johari and V. B. Shenoy, *ACS Nano* **6**, 5449 (2012).
- [52] H. Peelaers and C. G. Van de Walle, *Phys. Rev. B* **86**, 241401(R) (2012).
- [53] F. A. Rasmussen and K. S. Thygesen, *J. Phys. Chem. C* **119**, 13169 (2015).
- [54] S. Bertolazzi, J. Brivio, and A. Kis, *ACS Nano* **5**, 9703 (2011).
- [55] S.-H. Kang and Y.-K. Kwon, *Curr. Appl. Phys.* **19**, 690 (2019).
- [56] N. Lu, H. Guo, L. Li, J. Dai, L. Wang, W.-N. Mei, X. Wu, and X. C. Zeng, *Nanoscale* **6**, 2879 (2014).
- [57] P. Rivera, J. R. Schaibley, A. M. Jones, J. S. Ross, S. Wu, G. Aivazian, P. Klement, K. Seyler, G. Clark, N. J. Ghimire *et al.*, *Nat. Commun.* **6**, 6242 (2015).
- [58] E. Akbari, K. Jahanbin, A. Afroozeh, P. Yupapin, and Z. Buntat, *Phys. B: Condens. Matter* **545**, 510 (2018).
- [59] D. Saha, A. Varghese, and S. Lodha, *ACS Appl. Nano Mater.* **3**, 820 (2019).
- [60] S. Bhattacharyya and A. K. Singh, *Phys. Rev. B* **86**, 075454 (2012).